



## Design of a non-precious metal electrocatalyst for alkaline electrolyte oxygen reduction by using soybean biomass as the nitrogen source of electrocatalytically active center structures

Chao-Zhong Guo <sup>a, b,\*</sup>, Wen-Li Liao <sup>c</sup>, Chang-Guo Chen <sup>d,\*</sup>

<sup>a</sup> Research Institute for New Materials Technology, Chongqing University of Arts and Sciences, Yongchuan 402160, China

<sup>b</sup> Chongqing Key Laboratory of Environmental Materials & Remediation Technologies, Chongqing University of Arts and Sciences, Yongchuan 402160, China

<sup>c</sup> College of Materials and Chemical Engineering, Chongqing University of Arts and Sciences, Chongqing 402160, China

<sup>d</sup> College of Chemistry and Chemical Engineering, Chongqing University, Chongqing 400044, China



### HIGHLIGHTS

- An ORR electrocatalyst was prepared by using soybean biomass as the nitrogen source of active centers.
- The nitrogen in electrocatalysts is mainly the form of pyridinic and pyrrolic N species.
- The metallic Fe can facilitate the transformation of quaternary N to planar N during pyrolysis.
- The metallic Fe facilitates the joint incorporation of planar pyridinic and pyrrolic N into the carbon matrix.
- The content of planar N species plays an important role in improvement of the ORR activity in alkaline electrolyte.

### ARTICLE INFO

#### Article history:

Received 23 January 2014

Received in revised form

14 June 2014

Accepted 3 July 2014

Available online 11 July 2014

#### Keywords:

Oxygen reduction

ELECTrocatalyst

Soybean

Active site

Nitrogen source

### ABSTRACT

The development of less expensive, more active, and more stable catalyst substitute for Pt/C catalysts for oxygen reduction has recently become a hot topic. In this paper, we report a new strategy to design nitrogen-doped non-precious metal catalysts via the copyrolysis of metallic iron, soybean biomass, and carbon support at high temperatures. The results show that the nitrogen in electrocatalysts is mainly in the form of pyridinic and pyrrolic N species. The metallic Fe in the precursor can facilitate the transformation of quaternary N with a three-dimensional structure to planar pyridinic and pyrrolic N inside carbon matrix during pyrolysis, thereby improving the electrocatalytic activity of the prepared catalysts. We suggest that the planar N species may be the catalytically active center structures and may contribute to the enhancement of oxygen reduction reaction performance in an alkaline electrolyte. The prepared catalyst has superior tolerance against methanol crossover effect and outstanding stability compared with commercial Pt/C catalysts.

© 2014 Elsevier B.V. All rights reserved.

### 1. Introduction

Fuel cell-based systems show great potential as alternative power sources for a wide range of applications because of their high efficiency, high energy density, and low emissions [1]. Direct methanol alkaline fuel cells (DMAFCs) have advantages over polymer electrolyte membrane fuel cells because of the former's less

corrosive environment and more facile kinetics for the electro-reduction of oxygen molecules. However, a serious CO<sub>2</sub> poisoning problem precludes the development of alkaline fuel cells (AFCs) usually when a liquid electrolyte such as potassium hydroxide (KOH) aqueous solution is used. The development of alkaline solid polymer membranes instead of an alkaline solution can potentially simplify the AFCs and greatly reduce the carbonation problem [2,3]. In addition, the oxygen reduction reaction (ORR) on the cathode of AFCs has a pivotal function in controlling their performance because of the kinetic sluggishness of ORR in a complex four-electron transfer process [4]. Pt-based catalysts for ORR such as Pt/Au composites were developed for the Apollo lunar mission as early as the 1960s, but their large-scale commercial applications

\* Corresponding authors. Research Institute for New Material Technology, Chongqing University of Arts and Sciences, Yongchuan 402160, China. Tel./fax: +86 023 65111357.

E-mail addresses: [guochaozhong1987@163.com](mailto:guochaozhong1987@163.com) (C.-Z. Guo), [cgchen@cqu.edu.cn](mailto:cgchen@cqu.edu.cn) (C.-G. Chen).

have been hindered by high costs and scarcity of platinum [5]. Moreover, Pt-based catalysts are susceptible to time-dependent drift, and the high methanol crossover causes mixed potential in the cathode of fuel cells. Thus, many research efforts in the development of cathode catalysts have been focused mainly on decreasing Pt content or replacing Pt with less expensive materials [4,6].

Non-precious metal catalysts (NPMCs), especially pyrolyzed TM/N/C (TM = Fe, Co, Cu, etc.) systems, have been extensively studied as a low-cost catalyst alternative to Pt for ORR in acid or alkaline electrolytes in the past five decades [6–22]. However, none of these studies showed the necessary combination of activity and stability that could replace Pt-based catalysts in acidic fuel cells [13]. On the contrary, ORR kinetics are often more facile, and materials are more stable at alkaline environments [14]. For example, Meng et al. found that Fe/N/C catalysts exhibit enhanced activity and stability at alkaline conditions ( $\text{pH} = 13$ ) compared at acidic conditions ( $\text{pH} = 1$ ) [15]. Xi et al. similarly confirmed that Fe/N/C catalysts from the pyrolysis of hemin/C composites show superior ORR catalytic activity and stability in alkaline electrolyte than in acidic electrolyte [16]. These findings have significantly encouraged researchers to explore various materials that function as TM/N/C catalysts for ORR in alkaline media. Furthermore, selecting nitrogen sources to produce ORR active center structures has become a topic of interest because the nitrogen source is indispensable for TM/N/C catalyst synthesis, and an increase in the amount of nitrogen can effectively influence the amount of active sites [17]. Several nitrogen-containing precursors used in previous studies include purine and pyrimidine [10], polyaniline [18], phthalocyanine [19], amino acid [20], polypyrrole [21], and porphyrin [22]. TM/N/C catalysts with these nitrogen-rich molecules as nitrogen sources have reasonable ORR electrocatalytic activity, but their preparations are commonly carried out with complex procedures or expensive hardware. Exploring a facile method to prepare highly active and stable ORR catalysts remains a challenge.

We recently formed NPMCs for ORR at alkaline conditions by carbonizing blood proteins from animals [23–25]. Blood proteins are notably more inexpensive and abundant as opposed to Pt. Subsequently, we also developed another method for the formation of Fe/N/C catalysts from the precursors of transition metals, carbon black, and egg-white protein [26]. However, no systematic study on the carbonization behavior and functionalization of various bio-proteins has been conducted until now.

Soybeans are one of the most important crops grown in the United States [27]. They are abundantly and cheaply obtained; more than 250 million tons of soybeans are produced every year around the world, and they are sold for only ~550 U.S. dollars per ton. The content of soy proteins in soybean is commonly between 38% and 42%. In this study, we developed a novel method to prepare an inexpensive and active Fe/N/C catalyst (Fe/C–SOYB) by using nitrogen-rich soybean biomass as the specific nitrogen source for the active center structures. Fe/C–SOYB was carefully analyzed, and its ORR catalytic activity was evaluated in detail. Our results indicate that Fe/C–SOYB with high percentages of pyridinic and pyrrolic N substantially enhances the ORR electrocatalytic performance, thereby suggesting that this catalyst has a key function in the electrocatalysis of ORR at alkaline conditions.

## 2. Experimental

### 2.1. Materials and chemicals

Soybean (SOYB) was supplied by the Food Testing Center of Chongqing Bureau of Quality and Technology Supervision, China. Vulcan XC-72R commercial carbon black (V-CB,  $\phi = 30 \text{ nm}$ ) was

purchased from Cabot® and pretreated in  $4.5 \text{ mol l}^{-1} \text{ HNO}_3$  solution at  $80^\circ\text{C}$  for 12 h. The commercial Pt/C (20 wt.% Pt) catalyst was obtained from De Nora Elettrodi Co. Ltd., China. All other chemicals were of analytical grade and were obtained from Chongqing Chemical Reagent Co., China.

### 2.2. Catalyst preparation

First, 0.25 g of pretreated V-CB particles was dispersed well in  $\text{FeCl}_3$  solution (5.0 wt.% Fe), and the suspension was then magnetically stirred for 2 h and evaporated to about three-fourths of the liquid volume on a heating plate. Subsequently, it was completely dried overnight in an oven at  $100^\circ\text{C}$ . The obtained mixture was heat-treated in a tube furnace at  $900^\circ\text{C}$  for 1 h in  $\text{N}_2$  atmosphere to produce the Fe/C sample. SOYB was ball-milled with the yielded Fe/C particles (mass ratio of 2:1) for 0.5 h. The produced precursor was further treated in flowing  $\text{N}_2$  at  $900^\circ\text{C}$  for 2 h. The yielded sample is hereafter called Fe/C–SOYB.

To remove excess metal elements deposited on the support, Fe/C–SOYB was chemically treated with  $0.5 \text{ mol l}^{-1} \text{ H}_2\text{SO}_4$  solution at  $90^\circ\text{C}$  for 12 h. The sample obtained after acid-leaching is hereafter named Fe/C–SOYB-A. For the control sample, V-CB particles were first heat-treated at  $900^\circ\text{C}$  for 1 h in  $\text{N}_2$  atmosphere and then ball-milled with SOYB to form a precursor that does not contain transition metals. This precursor was further heat-treated at  $900^\circ\text{C}$  for 2 h to obtain the C–SOYB sample.

### 2.3. Characterization

X-ray diffraction (XRD) analysis was carried out using an X-ray diffractometer by Shimadzu XRD-6000 (Japan) with  $\text{Cu K}\alpha 1$  radiation ( $\lambda = 1.54178 \text{ \AA}$ ) at  $4^\circ \text{ min}^{-1}$ . X-ray photoelectron spectroscopy (XPS) analysis was performed using a VG Scientific ESCALAB 220 iXL spectrometer with an  $\text{Al K}\alpha$  ( $h\nu = 1486.69 \text{ eV}$ ) X-ray source. The total nitrogen content was determined using a Vario EL CUBE elemental analysis system (Germany). The morphology of the prepared samples was characterized via high-resolution scanning electron microscopy (SEM) (Ultra 55, Germany). Inductively coupled plasma-mass spectroscopy (ICP-MS) with an SCIEX ELAN DRCe ICP-MS system (PerkinElmer) was used to analyze the bulk composition of the prepared catalysts.

### 2.4. Electrochemical measurements

All electrochemical experiments were conducted using a CHI 600A electrochemical workstation (CH instruments, USA) at room temperature. A Pt wire and a  $\text{Hg}/\text{HgO}/1 \text{ mol l}^{-1} \text{ KOH}$  were used as the counter and reference electrodes, respectively. A rotation disk electrode (RDE) with a glass carbon (GC) electrode (5 mm in diameter, LKXZ-1, Tianjing Lanlike Electrochemical Instruments, China) was used as the working electrode. The modified-GC working electrode was fabricated by coating it with catalyst ink. Typically, 10  $\mu\text{l}$  of catalyst ink that is well dispersed in 0.5 wt.% Nafton/isopropanol solution was dropped onto the GC disk surface and then dried at room temperature. About 100  $\mu\text{g}$  of the catalysts, except Pt/C (29  $\mu\text{g}$ ), was loaded on the disk electrode. All the electrode potentials in this work are quoted versus a reversible hydrogen electrode (RHE).

All ORR activity measurements and methanol-tolerance tests were performed over a potential range of 1.15 V–0.15 V at a scan rate of  $5 \text{ mV s}^{-1}$  in  $\text{O}_2$ - or  $\text{N}_2$ -saturated  $0.1 \text{ mol l}^{-1} \text{ KOH}$  solution via cyclic voltammetry (CV) or linear sweep voltammetry. The onset potentials (the potential at which a current density of  $-100 \mu\text{A cm}^{-2}$  is recorded) were taken from the ORR polarization curves. The stabilities of Fe/C–SOYB and 20% commercial Pt/C were

also evaluated via an accelerated aging test (AAT). The AAT uses 5000 continuous potential cycles performed by scanning between 0.15 and 1.15 V at a scan rate of 50 mV s<sup>-1</sup> in 0.1 mol l<sup>-1</sup> KOH solution purged with N<sub>2</sub>. The ORR performance after AAT was further assessed using the same standard three-electrode cell described above.

### 3. Results and discussion

#### 3.1. Catalyst characterization

**Fig. 1a** shows the XRD patterns of C-SOYB, Fe/C, Fe/C-SOYB, Fe/C-SOYB-A, and V-CB. For C-SOYB, no other peaks were found aside from two amorphous carbon peaks centered at 2θ values of ~25° and ~44°, which are attributed to the graphitic planes (002) and (101), respectively [23]. The broad peak at 24° indicates the domination of the disordered carbon phase in C-SOYB, whereas the other weak broad peak at 44° suggests the existence of graphitic layers with small sizes and low three-dimensional order [25]. Compared with the 2θ value of V-CB, that of graphite (002) becomes smaller, and the width of the two diffraction peaks significantly increases, which may be influenced by the lower graphitization degree [17]. Fe/C-SOYB exhibits different phase

compositions, but the amorphous carbon phase is well preserved. The sharp peaks at 30.2°, 35.6°, 43.8°, 54.5°, 57.4°, and 63.8° can be ascribed to crystalline Fe<sub>2</sub>O<sub>3</sub> phases (PDF #39–1346). After the chemical treatment of Fe/C-SOYB with H<sub>2</sub>SO<sub>4</sub> solution, all of the crystalline phases were removed and were no longer observed in Fe/C-SOYB-A. In addition, Fe/C also exhibited two crystalline phase peaks centered at 2θ values of ~44.6° and ~65.0°, which are designated as the metallic α-Fe phases (110) and (200), respectively. The particle size of α-Fe in Fe/C composite is ≈ 25.6 nm, which was calculated using the Debye-Scherrer formula ( $D_{110} = k\lambda \times 57.32/\beta \cos\theta$ ) based on the (110) peak. The α-Fe particles were produced by the reduction of Fe (III) ions by V-CB in the pyrolysis process, and they further facilitated more catalytic structures to be formed, as confirmed by XPS analysis. However, they were re-oxidized by oxygen-containing fragments derived from the decomposed products of SOYB and produced a substantial number of Fe<sub>2</sub>O<sub>3</sub> phases in Fe/C-SOYB.

**Fig. 1b** shows the XPS analysis for the N1s region of the C–N bonding configuration and the corresponding distribution in C-SOYB, Fe/C-SOYB, and Fe/C-SOYB-A. The presence of nitrogen in the three catalysts clearly suggests that it was incorporated into the graphite structure of the prepared samples. The N1s spectrum can be deconvoluted into three peaks at ~398.8, ~400.0, and ~402.0 eV, which can be assigned to pyridinic N, pyrrolic N, and quaternary N, respectively [28–30]. The N/C ratios and fitting data are summarized in **Table 1**. The relative N/C ratio, which was determined via elemental analysis, was only 1.78% in C-SOYB but was 4.95% and 4.56% in Fe/C-SOYB and Fe/C-SOYB-A, respectively. These ratios indicate that the total nitrogen content during pyrolysis at high temperatures was significantly increased by the introduction of metallic iron, whereas nitrogen loss during the acid-leaching process was mainly induced by the protonation of pyridinic N species [31]. Among the three types of N atoms, only the pyridinic and pyrrolic forms, which have planar structures, have been proven to be active in ORR [32]. By contrast, quaternary N atoms, which possess a 3D structure, are not active in ORR. The low electrical conductivity of N-doped carbons with quaternary N atoms is caused by the interruption of their π–π conjugation by the 3D structure and largely contributes to the poor catalysis [33]. Therefore, the synthesis of N-doped carbons with more planar pyridinic and pyrrolic N atoms and fewer quaternary N atoms is essential for the fabrication of active catalysts. Heat treatment of the precursors with or without metallic Fe species mainly produces a high ratio of the pyrrolic N configuration. Pyrolyzing the precursors of carbon, nitrogen, and metallic iron at high temperatures led to an obvious increase in the percentage of pyridinic N from 24.8% for C-SOYB to 34.5% for Fe/C-SOYB. However, the percentage of quaternary N species decreased significantly. When Fe/C-SOYB was subjected to chemical leaching, it produced more pyrrolic N species (47.4% in total doped nitrogen), and the content of quaternary N species further decreased from 30.0% to 21.7%. These results clearly show that the large transformation of quaternary N to planar pyridinic and pyrrolic N occurs with iron doping or acid treatment. A little reduction in the percentage of pyridinic N inside

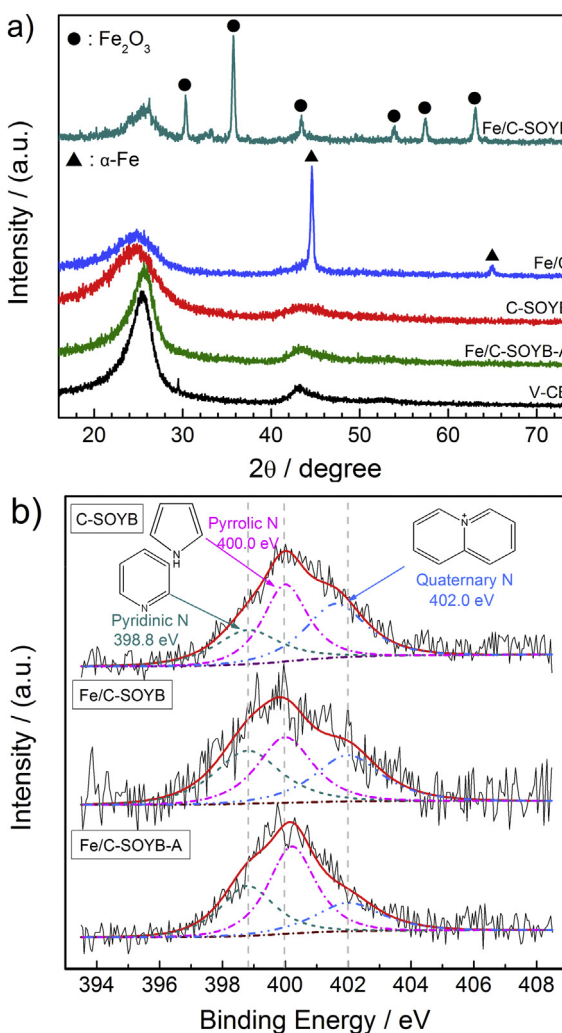


**Fig. 1.** (a) XRD patterns of V-CB, Fe/C, C-SOYB, Fe/C-SOYB and Fe/C-SOYB-A. (b) XPS spectra for the N1s region of C-SOYB, Fe/C-SOYB and Fe/C-SOYB-A.

**Table 1**

XPS data for the N1s region of C-SOYB, Fe/C-SOYB and Fe/C-SOYB-A from **Fig. 1(b)**.

Sample	N/C [%] <sup>[a]</sup>	Pyridinic N [%]	Pyrrolic N [%]	Quaternary N [%]	Planar N [%] <sup>[b]</sup>
C-SOYB	1.78	24.8	38.8	36.4	63.6
Fe/C-SOYB	4.95	34.5	35.5	30.0	70.0
Fe/C-SOYB-A	4.56	30.9	47.4	21.7	78.3

<sup>a</sup> The atomic ratio of N/C in three catalysts determined by elemental analysis.

<sup>b</sup> Total content of pyridinic- and pyrrolic-N species.

Fe/C-SOYB-A can be attributed to the formation of pyridinic-N-H (pyridinium) by the protonation of pyridinic N in 0.5 mol l<sup>-1</sup> H<sub>2</sub>SO<sub>4</sub> solution [31].

**Fig. 2** depicts high-resolution SEM images of Fe/C-SOYB before and after acid leaching in 0.5 mol l<sup>-1</sup> H<sub>2</sub>SO<sub>4</sub> solution. The carbon-based nanoparticles are  $\approx$  70 nm in size, which is larger than the particles of the carbon support (30 nm). The carbon support was covered and modified with thermally decomposed fragments of soy proteins inside the SOYB biomass, as confirmed by XPS analysis. Some crystalline agglomerations are observed only on the surface of Fe/C-SOYB, which can be attributed to the formation of Fe<sub>2</sub>O<sub>3</sub> phases. The concentrations of Fe/C-SOYB before and after chemical leaching were determined via ICP-MS. The results of the ICP-MS analysis show that the actual concentration of metal Fe decreases from 3.97 wt.% in Fe/C-SOYB to 0.29 wt.% in Fe/C-SOYB-A. These ratios suggest that most Fe particles were removed by chemical treatment with H<sub>2</sub>SO<sub>4</sub> solution, whereas residual metal Fe particles that survived the leaching treatment may be encased in the carbon structure [9].

### 3.2. Electrochemically catalytic activity

The electrocatalytic activities toward ORR were first evaluated via the CV method. As shown in **Fig. 3a**, compared with the featureless CV curve tested in N<sub>2</sub>-saturated KOH solution, the CV curve of Fe/C-SOYB tested in O<sub>2</sub>-saturated 0.1 mol l<sup>-1</sup> KOH solution shows a well-defined cathodic peak at 0.69 V, which is comparable with the peak potential of Pt/C catalyst (**Fig. 3b**). This result implies that Fe/C-SOYB exhibits ORR catalytic activity in alkaline

electrolyte. Furthermore, the crossover effects of methanol on ORR for both Fe/C-SOYB/GC and Pt/C/GC electrodes were also evaluated in O<sub>2</sub>-saturated 0.1 mol l<sup>-1</sup> KOH with methanol (5 mol l<sup>-1</sup>). As shown in **Fig. 3a**, no obvious change in ORR peak can be observed on the Fe/C-SOYB/GC electrode in O<sub>2</sub>-saturated electrolyte when methanol was added. However, for the Pt/C/GC electrode (**Fig. 3b**), when the electrolyte was changed from O<sub>2</sub>-saturated 0.1 mol l<sup>-1</sup> KOH aqueous solution to O<sub>2</sub>-saturated 0.1 mol l<sup>-1</sup> KOH + 5 mol l<sup>-1</sup> methanol aqueous solution, the ORR peak disappears and two typical oxidation peaks of methanol can be clearly observed. These results clearly indicate that Fe/C-SOYB has a notably higher selectivity toward ORR and better tolerance to crossover effect than Pt/C; thus, this catalyst has a potential application in DMAFCs without ion exchange membranes.

The ORR performance of GC electrode, V-CB, C-SOYB, Fe/C-SOYB, Fe/C-SOYB-A, and 20% commercial Pt/C was further studied via RDE. The large differences in the ORR catalytic activity are shown in **Fig. 4a**. All ORR catalytic activity data are summarized in **Table 2**. The GC electrode has poor activity for ORR, but C-SOYB exhibits better catalytic activity than V-CB because the structure of the carbon matrix is significantly changed by nitrogen doping, which produces a specific amount of pyridinic and pyrrolic N active species. The doping of nitrogen enhances the ability of graphene sheets inside the carbon matrix to donate electrons, which is advantageous for O<sub>2</sub> electroreduction [28]. Remarkably, Fe/C-SOYB exhibits the most onset potential ( $E_{\text{ORR}}$ ) of 0.84 V and half-wave potential ( $E_{1/2}$ ) of 0.68 V, which are lower than those of 20% Pt/C (0.95 and 0.85 V, respectively). A difference of  $\sim$ 170 mV on the  $E_{1/2}$  can be observed from the comparison of 20% Pt/C and Fe/C-SOYB. The  $E_{\text{ORR}}$  and  $E_{1/2}$  of Fe/C-SOYB are also lower than those of the catalyst (0.90 and 0.78 V, respectively) reported previously in literature [25]. However, Fe/C-SOYB exhibits the best ORR catalytic performance among the prepared catalysts on the basis of analyzing parameters such as  $E_{\text{ORR}}$ ,  $E_{1/2}$ , and the limited current densities in alkaline solution. Based on the XRD and XPS analysis results, the enhanced ORR activity of Fe/C-SOYB can be attributed to three aspects: (i) the metallic Fe in the precursor can facilitate the transformation of quaternary N to planar N and the increase in total nitrogen content; (ii) the metallic Fe can help to form new active structures on the modified carbons with other N-containing species created from the decomposition of SOYB in the pyrolysis process; and (iii) a high amount of the planar N species is produced in the Fe/C-SOYB catalyst.

To explore the function of metallic Fe in the formation of active sites, Fe/C-SOYB was chemically leached in 0.5 mol l<sup>-1</sup> H<sub>2</sub>SO<sub>4</sub> solution. The losses of  $E_{\text{ORR}}$  and  $E_{1/2}$  for the ORR of Fe/C-SOYB are only 10 and 20 mV, respectively, but the ORR current density of Fe/C-SOYB-A is higher than that of Fe/C-SOYB at 0.25 and 0.65 V. A slight decrease in the ratio of N/C for Fe/C-SOYB-A, which was caused by the transition of pyridinic N to pyridinic-N-H in an acid electrolyte, may have resulted in a lower  $E_{1/2}$  value. Moreover, the acid treatment of Fe/C-SOYB not only leads to large losses of transition metal particles but induces more catalytically active structures to be exposed on the surface, which leads to high active site density and improves the current density of Fe/C-SOYB-A. The increase in planar N percentage in Fe/C-SOYB-A, especially pyrrolic N, may have an important function in enhancing the limited current density. The Tafel slope of around 105 mV per decade, which was initially measured with Fe/C-SOYB in the range of 0.77 V–0.85 V (vs. RHE), remains virtually unchanged after acid leaching (**Fig. 4b**). In addition, the peak of Fe–N<sub>x</sub> centers were not found in the XPS spectrum for the N1s region of Fe/C-SOYB, which suggests that Fe–N<sub>x</sub> centers are not formed by nitrogen coordination in the presence of Fe. Therefore, we can reasonably speculate that the transition metal Fe may not be involved in catalytically

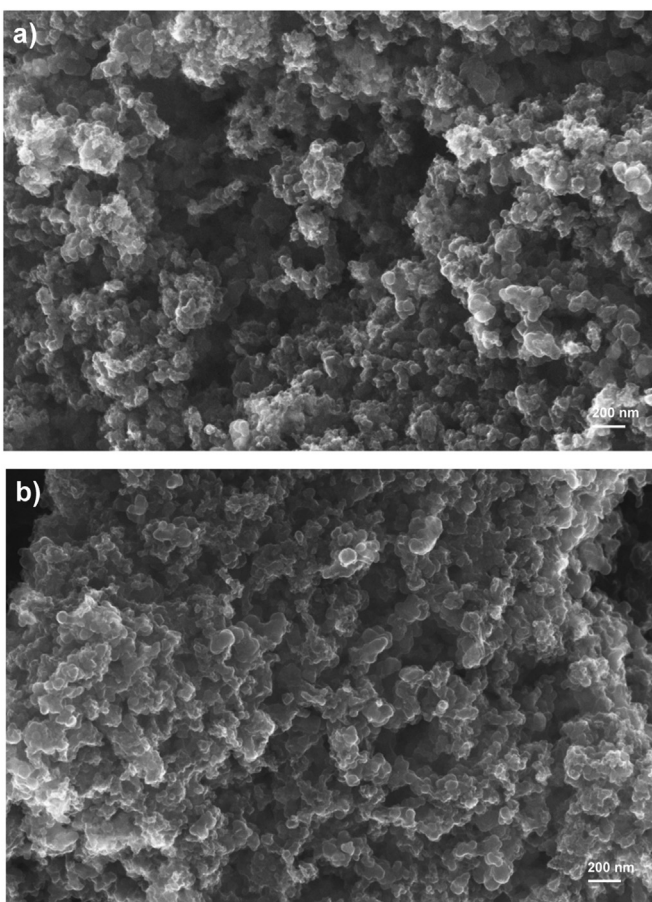


**Fig. 2.** High-resolution SEM images of Fe/C-SOYB (a) and Fe/C-SOYB-A (b) catalysts.

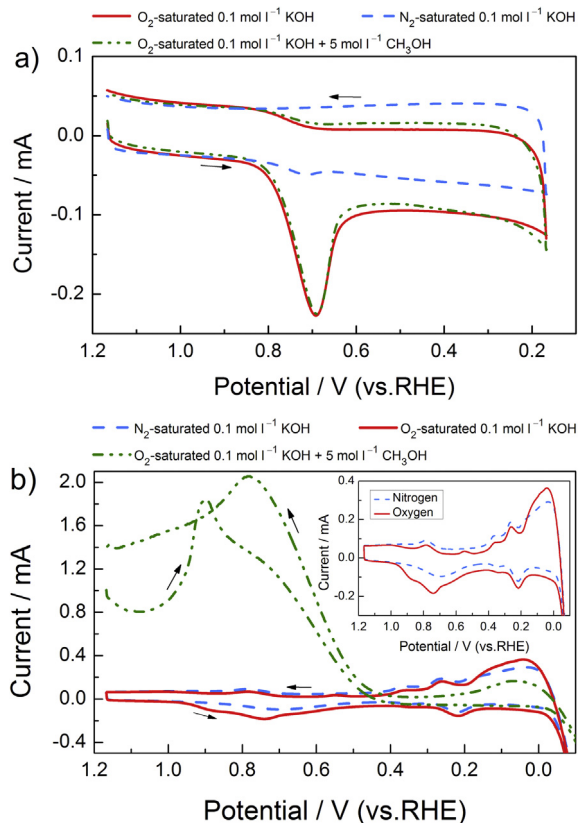


**Fig. 3.** Cyclic voltammograms of ORR on the (a) Fe/C-SOYB and (b) 20% Pt/C modified GC electrodes in  $N_2$ -saturated  $0.1 \text{ mol l}^{-1}$  KOH (dash),  $O_2$ -saturated  $0.1 \text{ mol l}^{-1}$  KOH (solid), and  $O_2$ -saturated  $0.1 \text{ mol l}^{-1}$  KOH +  $5 \text{ mol l}^{-1}$   $CH_3OH$  solutions (dash dot dot).

active structures, an assumption supported by previous reports [23,34]. Metallic Fe additives may be used as an agent to facilitate the incorporation of nitrogen within the carbon matrix [9].

The electrocatalytic activity of N-doped carbon-based electrocatalysts strongly depends on the nitrogen configurations, which are mainly pyrrolic or pyridinic type [29]. Pyridinic N refers to nitrogen atoms at the edge of graphene planes, each of which is bonded to two carbon atoms and donates one p-electron to the aromatic  $\pi$  system. Pyrrolic N refers to nitrogen atoms that are bonded to two carbon atoms and contribute to the  $\pi$  system with two p-electrons. The function of the real “catalytically active sites” remains controversial because their contribution to the catalytic activity is not well defined. Carbon atoms adjacent to nitrogen dopants possess a substantially high positive charge density to counterbalance the strong electronic affinity of the nitrogen atoms, which results in an enhanced adsorption of  $O_2$  and reactive intermediates that accelerate the ORR [35]. Several studies have proposed that the enhanced ORR electrocatalytic activity is attributed to pyridinic N and/or pyrrolic N [36,37]. A recent study has suggested that the pyrrolic N configuration is more important for the ORR performances of nitrogen-doped nanocarbons [25]. The electron-withdrawing effect of pyrrolic N can activate the adjacent carbon atoms and produce a net positive charge on neighboring carbons. This charge polarization assists the adsorption and reduction of the oxygen molecule on carbon atoms [38]. The results of electrochemical measurements and XPS analysis indicate that both planar pyridinic and pyrrolic N may be the N functionalities that are most responsible for the ORR electrocatalytic activity and may be the electrocatalytically active center structures for ORR.

Although Fe/C-SOYB shows ORR electrocatalytic activity and high methanol-tolerant performance comparable with the Pt/C catalyst, a good long-term stability is also a key factor for practical applications. Cycling durability tests in  $O_2$ -saturated  $0.1 \text{ mol l}^{-1}$  KOH solution over the potential range of  $1.15 \text{ V}$ – $0.15 \text{ V}$  were

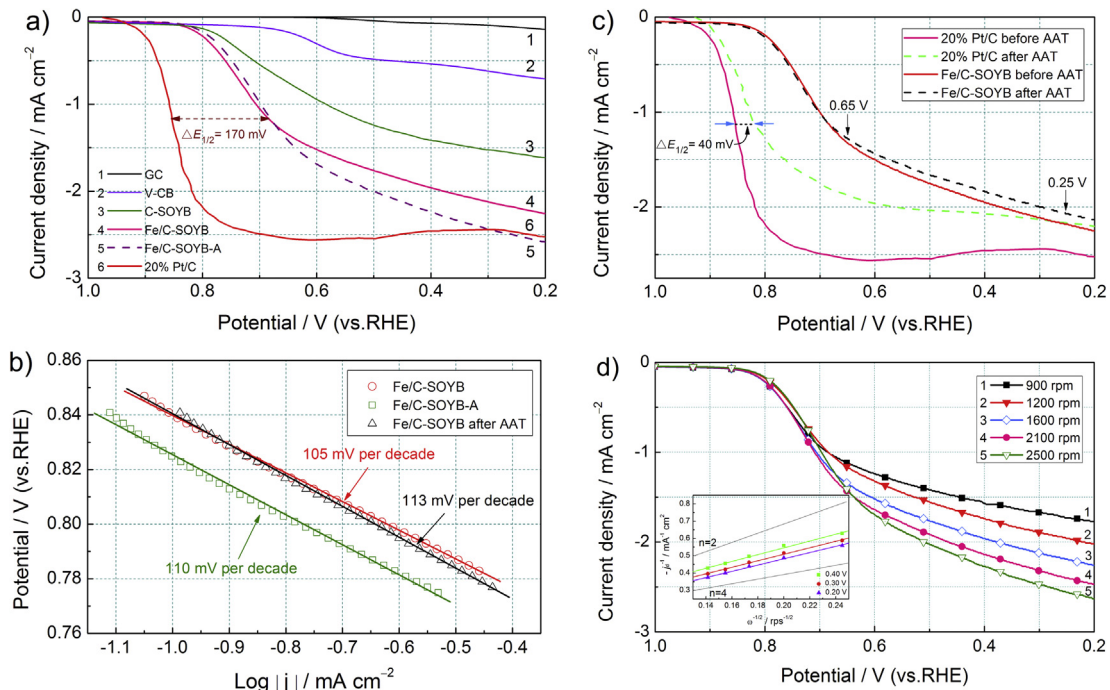


**Fig. 4.** (a) ORR polarization curves for GC electrode, V-CB, C-SOYB, Fe/C-SOYB, Fe/C-SOYB-A, and 20% Pt/C in  $O_2$ -saturated  $0.1 \text{ mol l}^{-1}$  KOH solution at a rotation rate of 1600 rpm. (b) Tafel plots for ORR on Fe/C-SOYB-A, and Fe/C-SOYB before and after AAT. Data are taken from (a). (c) ORR polarization curves for Fe/C-SOYB and 20% Pt/C catalysts before and after AAT in  $0.1 \text{ mol l}^{-1}$  KOH solution at a rotation rate of 1600 rpm. (d) ORR polarization curves for Fe/C-SOYB in  $O_2$ -saturated  $0.1 \text{ mol l}^{-1}$  KOH solution at different rotation rates. Inset is Koutecky-Levich plots of  $-j_d^{-1}$  vs.  $\omega^{1/2}$  obtained from (d).

**Table 2**

ORR electrocatalytic activity data from Fig. 4a for GC electrode, V-CB, C-SOYB, Fe/C-SOYB, Fe/C-SOVB-A and 20% Pt/C catalyst.

Sample	$E_{\text{ORR}}/\text{V}$	$E_{1/2}/\text{V}$	$J/\text{mA}^{-1}\text{cm}^{-2}$ @ 0.65 V	$J/\text{mA}^{-1}\text{cm}^{-2}$ @ 0.25 V
GC electrode	0.61	0.36	0.02	0.11
V-CB	0.74	0.57	0.15	0.65
C-SOYB	0.83	0.62	0.68	1.55
Fe/C-SOYB	0.84	0.68	1.27	2.18
Fe/C-SOVB-A	0.83	0.66	1.29	2.49
20% Pt/C	0.95	0.85	2.55	2.47

performed. Severe degradation of the commercial Pt/C catalyst compared with Fe/C-SOYB is shown by the decrease in the ORR performance (Fig. 4c). At 0.65 V, the current densities of Pt/C and Fe/C-SOYB catalysts before the AAT are 2.55 and 1.27 mA cm<sup>-2</sup>, respectively. After AAT, the Fe/C-SOYB catalyst retained 97% (1.23 mA cm<sup>-2</sup>) of the initial current density, whereas the Pt/C catalyst retained only 73% (1.87 mA cm<sup>-2</sup>) of the initial current density. Notably, the decrease in  $E_{\text{ORR}}$  and  $E_{1/2}$  for Pt/C catalyst is 30 and 40 mV, respectively, whereas the values of  $E_{\text{ORR}}$  and  $E_{1/2}$  for Fe/C-SOYB did not change significantly. An ORR Tafel slope measured with Fe/C-SOYB after AAT is around 113 mV per decade, which is similar to that with Fe/C-SOYB (Fig. 4b). A much lower degradation is observed for Fe/C-SOYB catalyst, which shows that it exhibits outstanding stability compared with 20% Pt/C catalyst. In addition, the stability of Fe/C-SOYB is also much better than that of Fe/N/C catalysts based on hemin [16], blood protein [25], and egg-white protein [26]. The outstanding stability of Fe/C-SOYB may be ascribed to four aspects: (i) it has catalytically active sites in the graphitic layers and strong interactions of the C–N covalent bonds; (ii) the surface properties of Fe/C-SOYB are maintained during potential cycling [39]; (iii) the nature of the N-doped active sites differs from that of Pt/C catalyst [25]; and (iv) silicates coming from the glass corrosion can block the active sites of Pt/C catalyst, thereby decreasing its stability [40].

RDE testing at different rotation rates was performed to understand the ORR mechanism of Fe/C-SOYB in KOH solution. The Koutecky–Levich (K-L) theory is applied to calculate the overall electron transfer number ( $n$ ) based on the fact that the ORR current densities depend on the electrode rotation rates in Fig. 4d. The diffusion-limited current density ( $j_d$ ) on RDE was estimated using the K-L equation (Eq. (1)) [41].

$$\frac{1}{j_d} = \frac{1}{j_k} + \frac{1}{0.62nFC_0D_0^{2/3}\nu^{-1/6}\omega^{1/2}} \quad (1)$$

where  $j_k$  is the kinetic current density of the ORR;  $F$  is the Faraday constant (96,485 C mol<sup>-1</sup>);  $C_0$  is the O<sub>2</sub> saturation concentration in the aqueous solution ( $1.2 \times 10^{-6}$  mol cm<sup>-3</sup>);  $D_0$  is the O<sub>2</sub> diffusion coefficient in 0.1 mol l<sup>-1</sup> KOH electrolyte ( $1.9 \times 10^{-5}$  cm<sup>2</sup> s<sup>-1</sup>);  $\nu$  is the kinetic viscosity of the solution (0.01 cm<sup>2</sup> s<sup>-1</sup>); and  $\omega$  is the electrode rotation rate (rpm). The K-L plots of  $-j_d^{-1}$  vs.  $\omega^{-1/2}$  for Fe/C-SOYB based on data at -0.5 V to -0.7 V are shown in the inset of Fig. 4d. For comparison, two theoretical lines for 2- and 4-electron transfer processes at fully diffusion-controlled conditions are also given. The K-L plots at various potentials exhibit good linearity and parallelism, which indicate first-order reaction kinetics for the ORR with regard to the concentration of dissolved oxygen. Based on the slope obtained from the K-L plots, the average  $n$  value for ORR at Fe/C-SOYB was ~3.1 at -0.5 V to -0.7 V, which suggests that the ORR catalyzed by the Fe/C-SOYB catalyst occurs via a mixed process of 2- and 4-electron transfer pathways but is dominated by a 4-electron transfer pathway to produce primarily H<sub>2</sub>O. Therefore, the

catalyst prepared in this work would be suitable for catalyzing the ORR in alkaline electrolytes.

#### 4. Conclusion

In this study, we developed a new method of designing Fe/N/C electrocatalysts with soybean biomass as the nitrogen source of electrocatalytically active center structures. Fe/C-SOYB contains a high percentage of the planar N species, which is promising for four-electron transfer in the ORR. Moreover, it clearly demonstrates ORR electrocatalytic activity, superior methanol-tolerant performance, and outstanding stability. The metallic iron or chemical leaching can facilitate the joint incorporation of planar pyridinic and pyrrolic N groups into a carbon matrix during pyrolysis at high temperatures. We propose that the planar N species could function as ORR active sites for the Fe/C-SOYB prepared in this work. Our study encourages the production of Fe/N/C catalysts with directional selection of nitrogen sources enriched with a high content of pyridinic and pyrrolic N species.

#### Acknowledgments

This work was supported by Natural Science Fund of China (Project No.21273292) and the Fundamental Research Funds for the Central Universities (Project No. CDJXS12220002). We gratefully thank Zhongli Luo, Zhongbin Li and Liangliang Tian for helpful discussions.

#### References

- [1] H.A. Gasteiger, S.S. Kocha, B. Sompalli, F.T. Wagner, *Appl. Catal. B* 56 (2005) 9–35.
- [2] F. Bidault, D.J.L. Brett, P.H. Middleton, N.P. Brandon, *J. Power Sources* 187 (2009) 39–48.
- [3] E. Antolini, E.R. Gonzalez, *J. Power Sources* 195 (2010) 3431–3450.
- [4] R. Othman, A.L. Dicks, Z. Zhu, *Int. J. Hydrogen Energy* 37 (2011) 357–372.
- [5] K. Gong, F. Du, Z. Xia, M. Durstock, L. Dai, *Science* 323 (2009) 760–764.
- [6] N.A. Karim, S.K. Kamarudin, *Appl. Energy* 103 (2013) 212–220.
- [7] R. Bashyam, P. Zelenay, *Nature* 443 (2006) 63–66.
- [8] I. Kruusenberg, L. Matisen, Q. Shah, A.M. Kannan, K. Tammeveski, *Int. J. Hydrogen Energy* 37 (2012) 4406–4412.
- [9] V. Nallathambi, J.W. Lee, S.P. Kumaraguru, G. Wu, B.N. Popov, *J. Power Sources* 183 (2008) 34–42.
- [10] J. Maruyama, N. Fukui, M. Kawaguchi, I. Abe, *J. Power Sources* 194 (2009) 655–661.
- [11] G. Liu, X. Li, P. Ganesan, B.N. Popov, *Electrochim. Acta* 55 (2010) 2853–2858.
- [12] J. Yan, H. Meng, F. Xie, X. Yuan, W. Yu, W. Lin, W. Ouyang, D. Yuan, *J. Power Sources* 245 (2014) 772–778.
- [13] A.A. Gewirth, M.S. Thorum, *Inorg. Chem.* 49 (2010) 3557–3566.
- [14] J.S. Spendelow, A. Wieckowski, *Phys. Chem. Chem. Phys.* 9 (2007) 2654–2675.
- [15] H. Meng, F. Jaouen, E. Proietti, M. Lefevre, J.P. Dodelet, *Electrochim. Commun.* 11 (2009) 1986–1989.
- [16] P.B. Xi, Z.X. Liang, S.J. Liao, *Int. J. Hydrogen Energy* 37 (2012) 4606–4611.
- [17] Z. Mo, R. Zheng, H. Peng, H. Liang, S. Liao, *J. Power Sources* 245 (2014) 801–807.
- [18] X. Fu, Y. Liu, X. Cao, J. Jin, Q. Liu, J. Zhang, *Appl. Catal. B Environ.* 130–131 (2013) 143–151.
- [19] L. Ding, J.L. Qiao, X.F. Dai, J. Zhang, J.J. Zhang, B.L. Tian, *Int. J. Hydrogen Energy* 37 (2012) 14103–14113.
- [20] J. Maruyama, N. Fukui, M. Kawaguchi, I. Abe, *J. Power Sources* 182 (2008) 489–495.
- [21] K.C. Lee, L. Zhang, H.S. Liu, R. Hui, Z. Shi, J.J. Zhang, *Electrochim. Acta* 54 (2009) 4704–4711.
- [22] S.N.S. Goubert-Renaudin, X.L. Zhu, A. Wieckowski, *Electrochim. Commun.* 12 (2010) 1457–1461.
- [23] C.Z. Guo, C.G. Chen, Z.L. Luo, *Int. J. Electrochem. Sci.* 8 (2013) 8940–8950.
- [24] C.Z. Guo, C.G. Chen, Z.L. Luo, *Chin. Sci. Bull.* 58 (2013) 3698–3703.
- [25] C.Z. Guo, C.G. Chen, Z.L. Luo, *J. Power Sources* 245 (2014) 841–845.
- [26] P. Liu, C.G. Chen, C.Z. Guo, M. Du, H.J. Wu, W. Yin, *Asian J. Chem.* 26 (2014) 2523–2526.
- [27] D.J. Myers, *Cereal Foods World* 38 (1993) 355–358.
- [28] Y. Shao, S. Zhang, M.H. Engelhard, G. Li, G. Shao, Y. Wang, J. Liu, I.A. Aksay, Y. Lin, *J. Mater. Chem.* 20 (2010) 7491–7496.
- [29] R. Liu, D. Wu, X. Feng, K. Müllen, *Angew. Chem. Int. Ed.* 49 (2010) 2565–2569.
- [30] E. Yoo, J. Nakamura, H. Zhou, *Energy Environ. Sci.* 5 (2012) 6928–6932.

- [31] X. Li, B.N. Popov, T. Kawahara, H. Yanagi, *J. Power Sources* 196 (2011) 1717–1722.
- [32] S. Yang, X. Feng, X. Wang, K. Müllen, *Angew. Chem.* 123 (2011) 5451–5455.
- [33] W. Ding, Z. Wei, S. Chen, X. Qi, T. Yang, J. Hu, D. Wang, L.J. Wan, S.F. Alvi, L. Li, *Angew. Chem. Int. Ed.* 52 (2013) 11755–11759.
- [34] Y.J. Si, C.G. Chen, W. Yin, H. Cai, *Chin. Chem. Lett.* 21 (2010) 983–986.
- [35] Y.Y. Shao, J.H. Sui, G.P. Yin, Y.Z. Gao, *Appl. Catal. B* 79 (2008) 89–99.
- [36] P.H. Matter, L. Zhang, U.S. Ozkan, *J. Catal.* 239 (2006) 83–96.
- [37] S. Maldonado, K.J. Stevenson, *J. Phys. Chem. B* 109 (2005) 4707–4716.
- [38] L. Yu, X. Pan, X. Cao, P. Hu, X. Bao, *J. Catal.* 282 (2011) 183–190.
- [39] H.T. Chung, J.H. Won, P. Zelenay, *Nat. Commun.* 4 (2013) 1922.
- [40] Y. Wang, Y. Liu, X. Lu, Z. Li, H. Zhang, X. Cui, Y. Zhang, F. Shi, Y. Deng, *Electrochem. Commun.* 20 (2012) 171–174.
- [41] A.J. Bard, L. Faulkner, *Electrochemical Methods*, second ed., Wiley & Sons, New York, 2001.